# Enhanced oxygen diffusivity in interfaces of nanocrystalline $ZrO_2$·$Y_2O_3$

**Gregor Knöner*†, Klaus Reimann*, Ralf Röwer*, Ulf Södervall‡, and Hans-Eckhardt Schaefer***

*Institut für Theoretische und Angewandte Physik, Universität Stuttgart, 70550 Stuttgart, Germany; and ‡Department of Microelectronics and Nanoscience, Chalmers University of Technology, 41926 Göteborg, Sweden

Communicated by Manuel Cardona, Max Planck Institute for Solid State Research, Stuttgart, Germany, February 10, 2003 (received for review November 20, 2002)

**First measurements of oxygen grain boundary diffusion coefficients in nanocrystalline yttria-doped $ZrO_2$ (n-$ZrO_2$·6.9 mol % $Y_2O_3$) are presented. The $^{18}O$ diffusion profiles measured by secondary ion mass spectroscopy are much deeper in the nanocrystalline specimens than in single crystals. An oxygen diffusivity, $D_B$, in the grain boundaries can be deduced, which is ≈3 orders of magnitude higher than in single crystals. From the present data the temperature variation of the oxygen grain boundary diffusivity, $D_B = 2.0 \times 10^{-5}$ exp ($-0.91$ eV/$k_BT$) m$^2$/s, and the oxygen surface exchange coefficient, $k = 1.4 \times 10^{-2}$ exp ($-1.13$ eV/$k_BT$) m/s, are derived.**

Yttria stabilized zirconia ($ZrO_2$·$Y_2O_3$) is widely used as an electrolyte material in solid oxide fuel cells or oxygen sensors. The technological importance of the material arises from its extraordinary oxygen transport properties, which are attributed to an oxygen vacancy mechanism. The replacement of quadrivalent Zr by trivalent Y gives rise to a high concentration of structural oxygen vacancies for charge compensation and stabilizes the cubic phase (1). The structural vacancies dramatically increase the mobility of oxygen ions, and the highest ionic conductivities were reported for $Y_2O_3$ concentrations of 7–10 mol % (2).

There is a broad interest in reducing the high operating temperatures of solid oxide fuel cells, typically 900–1,000°C, and resulting degradation effects by increasing the oxygen ion conductivity of the electrolyte. In undoped monoclinic nanocrystalline $ZrO_2$ it was found that the diffusion of oxygen in interfaces is $10^3$ to $10^4$ times faster than in the bulk of the crystallites (3). The question arises as to whether the high oxygen diffusivities of $ZrO_2$·$Y_2O_3$ upon doping can be further enhanced by the introduction of a large number of crystallite interfaces. A reason for an enhanced oxygen diffusion could be a loosely packed grain boundary structure, which is well established for pure metals (4), or easy formation of vacancy-type free volumes within the grain boundaries (5). On the other hand, there are reports that oxygen transport across grain boundaries could be impeded by a blocking effect due to space charge layers in the grain boundary region (6) or silica-containing grain boundary phases (7). In the present study, we present direct measurements of the grain boundary diffusion coefficients in nanocrystalline $ZrO_2$·$Y_2O_3$, which are accomplished by using $^{18}O$ as a tracer and secondary ion mass spectroscopy for depth profiling.

Fully dense nanocrystalline $ZrO_2$·$Y_2O_3$ bulk specimens were synthesized by dc sputtering of a ZrY metal target and crystallite condensation in an argon atmosphere at 240 Pa. Subsequent oxidation by slow exposure to an oxygen atmosphere (2,000 Pa) and *in situ* uniaxial compaction at high pressures (2 GPa) yielded disk-shaped specimens 5 mm in diameter with a relative mass density $\rho/\rho_0 \approx 89\%$ of the green body and a mean crystallite size <5 nm. From the sputter target with the composition of $Zr_{84}Y_{16}$, specimens with the final composition of $ZrO_2$·6.9 mol % $Y_2O_3$ were prepared.

Annealing in pure oxygen at atmospheric pressure at high temperatures led to a complete oxidation of the specimens, densification, and grain growth. Volume-averaged mean crystallite sizes $d = 65$ nm (1,000°C) and $d = 99$ nm (1,080°C) were determined from the broadening of the x-ray diffraction lines $\beta_k$ by a Rietveld fit by using Voigt functions (8–10). A qualitative analysis of the high indexed tetragonal (T) and cubic (C) reflections T{004}, C{400}, and T{220} at $2\Theta \approx 74°$ of the x-ray diffraction patterns revealed a cubic crystal structure of the nanocrystalline $ZrO_2$·6.9 mol % $Y_2O_3$ specimens after annealing (Fig. 1).

The sintering behavior and microstructure of the specimens were investigated by measurement of the mass density (Archimedes technique and geometrical studies), microporosimetry (11), and optical microscopy. After sintering at 1,000°C and 1,080°C, the annealing out of nanoscaled pores and an increase in mass density to $\rho/\rho_0 = 96\%$ were observed. In this state, a few microcracks were found between dense nanocrystalline agglomerates with a diameter of ≈100 $\mu$m (12). These cracks may contribute to a slightly increased $^{18}O$ background level (0.2%) in the $^{18}O$ diffusion profiles without further affecting the shape of the profiles (3).

Profiles of $^{18}O$ diffusion were measured on cubic nanocrystalline-$ZrO_2$·6.9 mol % $Y_2O_3$ specimens and single crystal $ZrO_2$·9.5 mol % $Y_2O_3$ specimens (Zirmat, North Billerica, MA). A specimen surface roughness of <10 nm in a surface area of $100 \times 100$ $\mu$m$^2$ was achieved by 1-$\mu$m diamond paste polishing. The diffusion anneals were performed in a 150-cm$^3$ quartz glass recipient at a 100-kPa pressure of $^{18}O$ in the temperature range between 200°C and 500°C. The temperature slopes of heating and cooling for the diffusion anneals were taken into account (13) for the determination of the diffusivities.

The $^{18}O$ diffusion profiles were measured by using the Cameca IMS-6f Secondary Ion Mass Spectroscopy facility at Chalmers University. Depth profiles were obtained by sputtering the specimen surface with a $Cs^+$ primary ion beam in an area of $250 \times 250$ $\mu$m$^2$ and analyzing the secondary ions emitted from the center of the crater (50 $\mu$m in diameter). A depth calibration was performed by measuring the crater depth with a surface profilometer and monitoring the Zr signal. The $^{18}O$ diffusion profiles were measured in both the nanocrystalline and the single crystal specimens for a direct comparison of the diffusion behavior and a precise determination of the volume diffusion coefficient $D_V$.

In the present case of high oxygen volume diffusivities $D_V$ in the $ZrO_2$·$Y_2O_3$ single crystals (see Fig. 2), the oxygen flux

$$-D_V \frac{\partial c(z)}{\partial z} = k(c_{gas} - c_S) \qquad [1]$$

is limited by the oxygen exchange across the gas/solid interface as determined by the rate constant $k$ (surface exchange coefficient) as well as the relative $^{18}O$ concentrations $c_{gas}$ in the gas

†To whom correspondence should be addressed. E-mail: gknoener@itap.physik.uni-stuttgart.de.

 www.pnas.org/cgi/doi/10.1073/pnas.0730783100

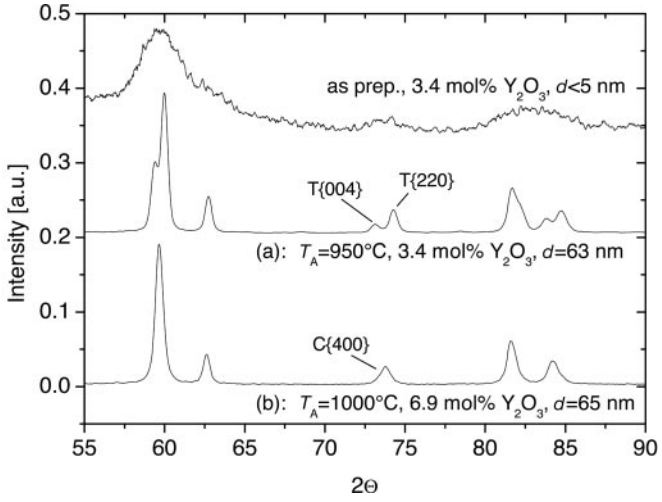


**Fig. 1.** The x-ray diffractograms of nanocrystalline $ZrO_2{\cdot}Y_2O_3$ specimens allow the determination of the crystallite size $d$ from the line broadening and a qualitative analysis of the crystal structure. Depending on the dopant concentration, tetragonal (*a*) and cubic (*b*) specimens, which can be distinguished by the C{400} reflection, were obtained after sintering at $T_A$. The cubic specimens were used for the diffusion experiments.

phase and $c_S$ at the surface of the solid. For this situation the $^{18}O$ diffusion profile

$$\frac{c(z)-c_0}{c_{gas}-c_0} = \mathrm{erfc}\left(\frac{z}{2\sqrt{Dt}}\right) - \exp(hz+h^2Dt)\cdot\mathrm{erfc}\left(\frac{z}{2\sqrt{Dt}}+h\sqrt{Dt}\right) \quad [2]$$

has been derived (14) with $h = k/D$. From a fit of Eq. **2** to the $^{18}O$ profile $c(z)$, the $^{18}O$ background level $c_0$, the exchange rate $k$, and the volume $^{18}O$ diffusivity $D_V$ can be determined.

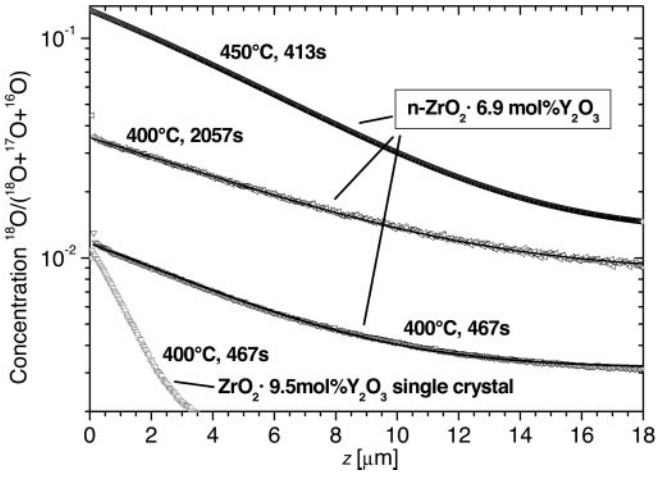


**Fig. 2.** Diffusion profiles of oxygen self-diffusion in a $ZrO_2{\cdot}9.5$ mol % $Y_2O_3$ single crystal with a (100) surface and in nanocrystalline $ZrO_2{\cdot}Y_2O_3$ measured by secondary ion mass spectroscopy. The diffusion anneals were carried out in a 10-kPa, 97% enriched $^{18}O$ atmosphere at the temperatures and times indicated. The deeper penetration of the tracer in nanocrystalline specimens compared with single crystals indicates faster effective diffusion due to the large volume fraction of grain boundaries. The shape of the profiles is typical for diffusion from a constant source under type A kinetics (see text) with a limited gas exchange at the specimen surface.

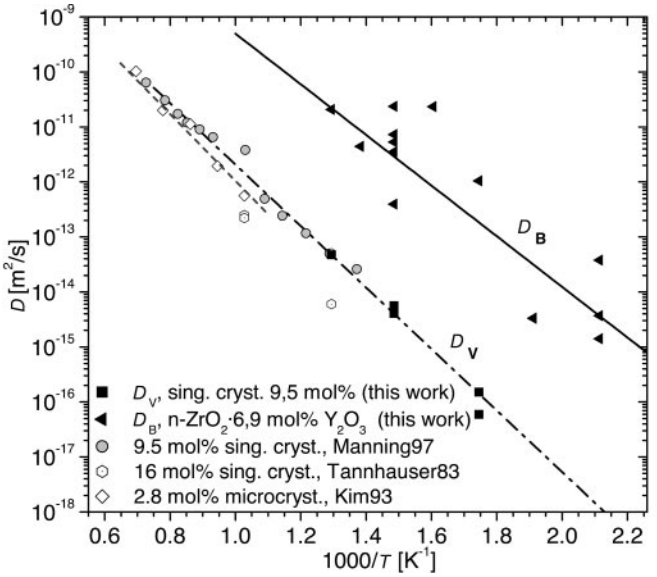


**Fig. 3.** Volume and interface diffusion coefficients of $^{18}O$ in $ZrO_2{\cdot}Y_2O_3$ and comparison with data from literature (15–17). The diffusion in the interfaces of nanocrystalline $ZrO_2{\cdot}6.9$ mol % $Y_2O_3$ is 3 orders of magnitude faster than in the bulk of single crystal $ZrO_2{\cdot}9.5$ mol % $Y_2O_3$. The activation enthalpies of (1.11 ± 0.06) eV for volume diffusion and (0.91 ± 0.2) eV for grain boundary diffusion were derived.

The study of $ZrO_2{\cdot}9.5$ mol % $Y_2O_3$ single crystals with a (100) surface extends the earlier data for $D_V$ (15–17) to lower temperatures. An activation enthalpy $H_V = (1.11 \pm 0.06)$ eV, in agreement with the value of the conductivity measured by impedance spectroscopy (18), together with a pre-exponential factor $D_{0V} = 0.8 \times 10^{-6}$ m$^2$/s is derived by fitting the Arrhenius equation

$$D = D_0{\cdot}\exp(-H/k_BT) \quad [3]$$

to the volume diffusion coefficients $D_V$ (see Fig. 3); $k_B$ denotes the Boltzmann constant.

A much higher $^{18}O$ diffusivity in the nanocrystalline $ZrO_2{\cdot}6.9$ mol % $Y_2O_3$ specimens than in the single crystals is evidenced by the deeper penetration of the diffusion profiles at 400°C shown in Fig. 2. We assume a type A diffusion behavior because the volume diffusion length $\sqrt{D_Vt}$ is much larger than the crystallite size $d < 100$ nm (19, 20). In this case, simultaneous contributions from the grains ($D_V$) and the grain boundaries ($D_B$) yield an effective diffusivity

$$D_{eff} = (1-f)D_V + fD_B, \quad [4]$$

which is obtained from the diffusion profiles by a fit of Eq. **2**. The volume fraction $f = 2\delta/d$ of grain boundaries is characterized by the grain size $d$ and the grain boundary width $\delta \approx 0.5$ nm (21, 22) and is used together with the above $D_V$ values from the above oxygen diffusion measurements on $ZrO_2{\cdot}9.5$ mol % $Y_2O_3$ single crystals to deduce the grain boundary diffusion coefficients $D_B$.

We use these $D_V$ values for the oxygen volume diffusivity in the nanocrystalline specimen irrespective of the fact that the composition is slightly different in the single crystal and the nanocrystalline specimens. This idea is reasonable because in this composition range the ion conductivity in $ZrO_2{\cdot}Y_2O_3$ single crystals is observed to be practically independent of composition (2, 18).

The scattering of the $D_B$ values (Fig. 3) originates from structural differences between the specimens, e.g., differences in agglomeration and crack formation during sintering, and inho-

PHYSICS

mogeneities within the specimen, e.g., an inhomogeneous grain size distribution, resulting in a small dependence of the profile on the analysis spot. An enhancement of the specimen homogeneity could be reached by ultrasonic treatment of the nanostructured powder before compaction to avoid particle agglomeration. Experiments involving diffusion under high $^{18}O$ pressure to enhance the signal-to-background ratio of the tracer are in preparation.

The grain boundary oxygen diffusivity $D_B = 2.0 \times 10^{-5}$ exp $(-0.91\ \text{eV}/k_BT)$ $m^2/s$ is deduced to be by 3 orders of magnitude higher than the volume diffusivity $D_V = 8.0 \times 10^{-7}$ exp $(-1.11\ \text{eV}/k_BT)$ $m^2/s$ (see Fig. 3). This finding may indicate that the concentration and/or the mobility of the oxygen vacancies in the interfaces are even higher than in doped single crystals.

A high oxygen diffusivity in grain boundaries as measured here can be deduced from structural studies as discussed in the following. Specific information on the atomic structure of $ZrO_2$·10 mol % $Y_2O_3$ grain boundaries has recently been obtained by analytical high-resolution transmission electron microscopy (23, 24). Making use of Z-contrast imaging and electron energy-loss spectroscopy (EELS) on a symmetric 24° [001] tilt boundary an increase of the yttrium concentration in the grain boundary core by about a factor of 2 has been found, as anticipated by early auger electron spectroscopy/x-ray photoelectron spectroscopy (25) and energy dispersive x-ray spectroscopy (22) studies. A concomitant increase in the concentration of oxygen vacancies exceeding the value expected from the enhanced yttrium concentration has been observed in agreement with atomic simulations of the grain boundary (23). From the excess oxygen vacancies and the EELS studies it is furthermore concluded that there are 1.45 free electrons per formula unit available in the grain boundary.

In high-resolution electron micrographs of $ZrO_2$·$Y_2O_3$ films with 10–15 mol % $Y_2O_3$ narrow grain boundaries (≈0.5 nm) with free volumes are observed (26). In the vicinity of the grain boundary stacking faults or distortions of adjacent lattice planes may further contribute to an enhancement of the concentration and mobility of free volumes for oxygen transport. This enhancement may also occur as a consequence of the increased mean square displacement of oxygen ions obtained from molecular dynamics studies of a Σ5 twist boundary (27).

Furthermore, the activation enthalpy $H_B = (0.91 \pm 0.2)$ eV of the grain boundary oxygen diffusivity observed here seems to be reduced in comparison to the value $H_V = (1.11 \pm 0.06)$ eV for volume diffusion, which indicates an enhanced mobility of the oxygen ions in $ZrO_2$·$Y_2O_3$ grain boundaries. The activation enthalpy $H_B$ clearly does not exceed the value $H_V$ as expected from the behavior of the oxygen activation enthalpy in bulk crystals (18), which increases with yttrium concentration. Thus, the reduction within the yttrium-rich grain boundary originates from structural modifications.

Conventionally the oxygen diffusivity $D$ is correlated to the ion conductivity $\sigma$, as investigated by impedance spectroscopy, via the Nernst–Einstein relationship

$$\sigma = \frac{(\alpha e)^2 n_{O^{2-}}}{f_D k_B T} D, \qquad [5]$$

where $e$ denotes the electronic charge, $\alpha$ the charge number of the diffusing species, $n_{O^{2-}}$ the atomic concentration of the diffusing $O^{2-}$ ions, and $f_D$ a correlation factor. Making use of the oxygen diffusivities $D_V$ measured in $ZrO_2$·$Y_2O_3$ single crystals (15) or in the present study together with the bulk conductivity $\sigma_V$ (15, 18), reasonable values of $\alpha = 2$ and $f_D = 0.33$ can be deduced. It is unclear whether Eq. **5** holds for the case of oxygen diffusion in grain boundaries or whether it should be modified and further studies are required. The oxygen diffusivity in grain boundaries is enhanced by a factor of 1,000 beyond that of bulk crystals as shown above, whereas the ion conductivity is reduced (6, 28), reportedly due to interfacial space charges (6, 29). Yet, with decreasing grain size, the specific conductivity of grain boundaries is reported to increase (28), but not beyond the bulk conductivity $\sigma_V$. For elucidating the correlation between the diffusivity and the conductivity in grain boundaries, measurements of the ion conductivity in the same specimens as used for the present diffusion experiments are required.

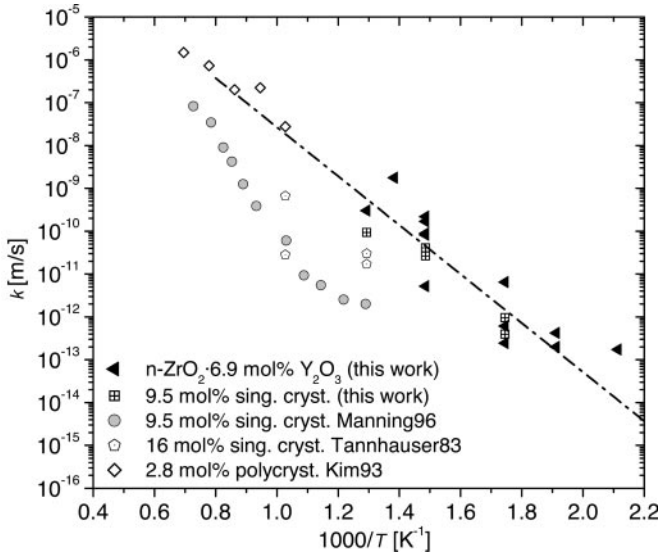


**Fig. 4.** Surface exchange coefficients $k$ for $^{18}O$ exchange at the surface of $ZrO_2$·$Y_2O_3$ and comparison with data from literature (15–17). The slow gas exchange leads to low tracer concentrations at the surface. An activation enthalpy for the exchange process of $H_k = 1.13$ eV is derived from the temperature dependence of $k$.

In the case of the high interfacial oxygen diffusivity demonstrated here, a high surface oxygen exchange rate is of additional importance for future experiments. The surface exchange coefficient $k$ derived from a fit of Eq. **2** to the diffusion profiles in nanocrystalline $ZrO_2$·6.9 mol% $Y_2O_3$ does not significantly differ from the values for $ZrO_2$·9.5 mol % $Y_2O_3$ single crystals. From this similarity we conclude that the exchange coefficient for oxygen at the grain boundaries is not significantly different from that for the bulk surface. The temperature variation $k = 1.4 \times 10^{-2}$ exp $(-1.13\ \text{eV}/k_BT)$ m/s of the exchange coefficient (see Fig. 4) for the present nanocrystalline $ZrO_2$·6.9 mol % $Y_2O_3$ specimens gives an activation enthalpy of 1.13 eV, similar to the value derived from the present experiments on $ZrO_2$·9.5 mol % $Y_2O_3$ single crystals and to the values for microcrystalline $ZrO_2$·2.8 mol % $Y_2O_3$ (17). The much lower exchange coefficients reported for (100) surfaces of $ZrO_2$·9.5 mol % $Y_2O_3$ single crystals (15) may originate from different surface structure and pretreatment.

In conclusion, we point out that in the present studies of the oxygen diffusivity $D_B$ in nanocrystalline $ZrO_2$·6.9 mol % $Y_2O_3$ oxygen diffusivities in grain boundaries enhanced by a factor of 1,000 have been observed with a temperature dependence according to $D_B = 2.0 \times 10^{-5}$ exp $(-0.91\ \text{eV}/k_BT)$ $m^2/s$. For promising future applications of this high oxygen diffusivity an enhancement of the oxygen surface exchange coefficient $k = 1.4 \times 10^{-2}$ exp $(-1.13\ \text{eV}/k_BT)$ m/s is desirable.

The valuable technical assistance in the specimen preparation and the chemical analysis by H. Wendel and A. Maier, Max-Planck-Institut für Metallforschung, Stuttgart, is gratefully acknowledged. This work was supported by Deutsche Forschungsgemeinschaft Grant Scha428/30-1.

1. Eichler, A. (2001) *Phys. Rev. B Condens. Matter* **64,** 1–8.
2. Strickler, D. W. & Carlson, W. G. (1964) *J. Am. Ceram. Soc.* **47,** 122–127.
3. Brossmann, U., Würschum, R., Södervall, U. & Schaefer, H.-E. (1999) *J. Appl. Phys.* **85,** 7646–7654.
4. Schaefer, H.-E., Reimann, K., Straub, W., Phillipp, F., Tanimoto, H., Brossmann, U. & Würschum, R. (2000) *Mater. Sci. Eng. A* **286,** 24–28.
5. Würschum, R., Shapiro, E., Dittmar, R. & Schaefer, H.-E. (2000) *Phys. Rev. B Condens. Matter* **62,** 12021–12027.
6. Guo, X. & Maier, J. (2001) *J. Electrochem. Soc.* **148,** E121–E126.
7. Badwal, S. P. S. (1995) *Solid State Ionics* **76,** 67–80.
8. Reimann, K., Fecht, H.-J. & Schaefer, H.-E. (2001) *Scri. Mater.* **44,** 1999–2003.
9. Rietveld, H. M. (1969) *J. Appl. Crystallogr.* **2,** 65–71.
10. Reimann, K. & Würschum, R. (1997) *J. Appl. Phys.* **81,** 7186–7192.
11. Brunauer, S., Emmett, P. H. & Teller, E. (1938) *J. Am. Chem. Soc.* **60,** 309–319.
12. Knöner, G. (2002) Master Thesis (University of Stuttgart, Stuttgart).
13. Killoran, D. R. (1962) *J. Electrochem. Soc.* **190,** 170–171.
14. Crank, J. (1957) *The Mathematics of Diffusion* (Oxford Univ. Press, London), pp. 30–35.
15. Manning, P. S., Sirman, J. D., Souza, R. A. & Kilner, J. A. (1997) *Solid State Ionics* **100,** 1–10.
16. Tannhauser, D. S., Kilner, J. A. & Steele, B. C. H. (1983) *Nucl. Instrum. Methods* **218,** 504–508.
17. Kim, B.-K., Park, S.-J. & Hamaguchi, H. (1993) *J. Am. Ceram. Soc.* **76,** 2119–2122.
18. Filal, M., Petot, C., Mokchah, M., Chateau, C. & Carpentier, J. L. (1995) *Solid State Ionics* **80,** 27–35.
19. Fisher, J. C. (1951) *J. Appl. Phys.* **22,** 74–79.
20. Harrison, L. G. (1961) *Trans. Faraday Soc.* **57,** 1191–1199.
21. Nitsche, R., Rodewald, M., Skandan, G., Fuess, H. & Hahn, H. (1996) *Nanostruct. Mater.* **7,** 535–546.
22. Merkle, K. L., Bai, G.-R., Li, Z., Song, C.-Y. & Thompson, L. J. (1998) *Phys. Status Solidi A* **166,** 73–89.
23. Lei, Y., Ito, Y. & Browning, N. D. (2002) *J. Am. Ceram. Soc.* **85,** 2359–2363.
24. Dickey, E. C. & Fan, X. (2001) *J. Am. Ceram. Soc.* **84,** 1361–1368.
25. Theunissen, G. S. A. M., Winnubst, A. J. A. & Burggraaf, A. J. (1992) *J. Mater. Sci.* **27,** 5057–5066.
26. Merkle, K. L., Thompson, L. J., Bai, G.-R. & Eastman, J. A. (2001) *MRS Symp. Proc.* **654,** AA1.6.1–AA1.6.6.
27. Fisher, C. A. J. & Matsubara, H. (1999) *J. Eur. Ceram. Soc.* **19,** 703–707.
28. Mondal, P., Klein, A., Jaegermann, W. & Hahn, H. (1999) *Solid State Ionics* **118,** 331–339.
29. Guo, X. (1995) *Solid State Ionics* **81,** 235–242.